remote sensing

MDPI

Article

Analysis of Macro- and Microphysical Characteristics of Ice Clouds over the Tibetan Plateau Using CloudSat/CALIPSO Data

Yating Guan [1,2,†], Xin Wang [1,3,*], Juan Huo [1,3], Zhihua Zhang [1,†], Minzheng Duan [1,3] and Xuemei Zong [1]

[1] Key Laboratory of Middle Atmosphere and Global Environment Observation, Institute of Atmospheric Physics, Chinese Academy of Sciences, Beijing 100029, China; guanyating20@mails.ucas.ac.cn (Y.G.); huojuan@mail.iap.ac.cn (J.H.); zhangzhihua@mail.iap.ac.cn (Z.Z.); dmz@mail.iap.ac.cn (M.D.); zongxm@mail.iap.ac.cn (X.Z.)
[2] Aerospace Newsky Technology Co., Ltd., Beijing 100854, China
[3] College of Earth and Planetary Sciences, University of Chinese Academy of Sciences, Beijing 100049, China
* Correspondence: wangx2003@mail.iap.ac.cn
† These authors contributed equally to this work.

Abstract: Utilizing CloudSat/CALIPSO satellite data and ERA5 reanalysis data from 2007 to 2016, this study analyzed the distributions of optical and physical characteristics and change characteristics of ice clouds over the Tibetan Plateau (TP). The results show that the frequency of ice clouds in the cold season (November to March) on the plateau is over 80%, while in the warm season (May to September) it is around 60%. The average cloud base height of ice clouds in the warm season is 3–5 km, and mostly around 2 km in the cold season. The average cloud top height in the warm season is around 5–8 km, while in the cold season it is mainly around 4.5 km. The average thickness of ice clouds in both seasons is around 2 km. The statistical results of microphysical characteristics show that the ice water content is around 10^{-1} to 10^{3} mg/m^3, and the effective radius of ice clouds is mainly in the range of 10–90 μm. Both have their highest frequency in the west of the TP and lowest in the northeast. A comprehensive analysis of the change in temperature, water vapor, and ice cloud occurrence frequency shows that the rate of increase in water vapor in the warm season is greater than that in the cold season, while the rates of increase in both surface temperature and ice cloud occurrence are smaller than in the cold season. The rate of increase in temperature in the warm season is around 0.038 °C/yr, and that in the cold season is around 0.095 °C/yr. The growth rate of thin ice clouds in the warm season is around 0.15% per year, while that in the cold season is as high as 1% per year. The results suggest that the surface temperature change may be related to the occurrence frequency of thin ice clouds, with the notable increase in temperature during the cold season possibly being associated with a significant increase in the occurrence frequency of thin ice clouds.

Keywords: Tibetan Plateau; ice clouds; CloudSat; plateau warming

check for updates

Citation: Guan, Y.; Wang, X.; Huo, J.; Zhang, Z.; Duan, M.; Zong, X. Analysis of Macro- and Microphysical Characteristics of Ice Clouds over the Tibetan Plateau Using CloudSat/CALIPSO Data. *Remote Sens.* **2024**, *16*, 3983. https://doi.org/10.3390/rs16213983

Academic Editor: Carmine Serio

Received: 28 August 2024
Revised: 12 October 2024
Accepted: 23 October 2024
Published: 26 October 2024

Copyright: © 2024 by the authors. Licensee MDPI, Basel, Switzerland. This article is an open access article distributed under the terms and conditions of the Creative Commons Attribution (CC BY) license (https://creativecommons.org/licenses/by/4.0/).

1. Introduction

As an important meteorological element, clouds play a pivotal role in regulating Earth's radiation balance, global energy distribution, and hydrological cycle [1,2]. They also affect the dynamic and thermodynamic processes of the atmosphere, thus occupying a significant position within the Earth–atmosphere system. According to the different particle states within clouds, cloud layers can be classified into three distinct types: ice clouds, water clouds, and mixed clouds. Ice clouds are composed of irregularly shaped ice crystal particles, covering around 20–30% of the world [3]. The horizontal and vertical distribution of ice clouds can affect the Earth–atmosphere system, affecting global radiation, weather, and climate change [4–6]. Due to the intricate formation processes of ice clouds, the vertical distribution of ice crystal sizes and ice water content (IWC) exhibits significant nonuniformity, posing numerous challenges to their detection [7]. The fourth report of the Intergovernmental Panel on Climate Change pointed out that there are large uncertainties

in the role of ice clouds in radiative forcing and climate change, mainly due to significant differences in numerical simulations of ice cloud parameters between different climate models [8–10].

The Tibetan Plateau (TP), also often referred to as the "third pole of the world", is the highest and most complex plateau in the world. The unique topography of the plateau and its strong non-adiabatic heating significantly affect the Asian monsoon system and the atmospheric circulation in the Northern Hemisphere [11–13]. Because of the existence of the plateau monsoon, the climate differences between the east and west sides of the TP, as well as the south and north sides, are highly unique globally, forming a distinctive plateau climate region [14]. An in-depth understanding of ice cloud structure and distribution over the TP is of great significance for studying global and regional weather and climate change. Previously, researchers have used active satellite data to analyze the structure and distribution of ice clouds over the plateau. Zhao et al. [15] used CloudSat data to study the cloud water path and radar reflectivity over the plateau and found that the central, northern, and western regions of the TP have high liquid water paths, with ice clouds as the main source. The radar reflectivity ranges from −27 to 17 dBZ, concentrated within 3–9 km. Liu et al. [16] used CloudSat data to study the frequency, distribution characteristics, and physical causes of eight types of clouds at different heights over the plateau, and found that compared with low and medium clouds, high clouds have the lowest frequency and mainly occur in the southern part of the plateau in summer. Kukulies et al. [17] analyzed the vertical structure of various cloud systems and their seasonal and diurnal variation characteristics over the TP based on CloudSat and CALIPSO and found that the occurrence frequency of ice clouds is significantly larger than that of water clouds and mixed clouds. Moreover, the diurnal variations of ice clouds are smaller than the effect of seasonal variations.

In the context of global warming, the significant warming of the TP has sparked widespread discussion [12,18–20]. In addition to the impact of human activities and increased greenhouse gas emissions [21], the distribution of and changes in clouds also have a significant impact on plateau warming. Duan and Wu [22] showed that climate warming over the TP may be related to the decrease in total and low-cloud cover. Pan et al. [23] pointed out that low-cloud cover and geometric thickness over the plateau region decreased by around 4.2% and 130 m, respectively, between 2007 and 2015, resulting in an increase in surface shortwave radiation of around 29.7 W/m^2, while longwave changes were not significant, thus promoting the warming of the plateau. Bao et al. [24] revealed that daytime water vapor changes over the plateau can lead to changes in cloud cover, and the cooling effect of cloud cover can affect temperature changes, which are more pronounced in summer. The above research, however, focuses mainly on total cloud and low-cloud cover, while research on ice clouds is relatively scarce. Due to the relative transparency of ice clouds towards incident solar shortwave radiation, they primarily exert a net warming effect through absorbing infrared radiation emitted from Earth's surface and the atmosphere beneath the clouds [25,26]. Hua et al. [27] found that the warming rate in the cold season of the TP was more notable than that in the warm season from 2000 to 2015. The decrease in mid-level cloud albedo and the increase in the high-cloud longwave greenhouse effect may have contributed to the persistent warming phenomenon during the cold season of the plateau. Wang et al. [28] found through their study of different-phase clouds over the plateau that ice clouds dominate the radiation effect inside the atmosphere, with radiation contributions of up to 80% and 40% in the cold and warm seasons [28]. Thus, it is of great significance to study the distribution and change characteristics of ice clouds in plateau areas.

This study is based on CloudSat/CALIPSO satellite data and ERA5 reanalysis data, to analyze the distributions of optical and physical characteristics of ice clouds over the TP and their change attributes, so as to further understand their spatial distribution and temporal variation and provide a more accurate data reference and basis for improving the

parameterization schemes of ice cloud models over this region and enhance the precision of model predictions.

2. Data and Methods

The CloudSat and CALIPSO satellites were launched on 28 April 2006, and together they joined the A-Train constellation, with a temporal separation of only 15 s. The two satellites orbit the Earth at an altitude of approximately 700 km, circling the planet 13 to 16 times each day and completing a full global observation approximately every 14 days. CloudSat (http://www.cloudsat.cira.colostate.edu/, accessed on 10 November 2023) carries a Cloud Profiling Radar (CPR) operating at a frequency of 94 GHz/3 mm, while CALIPSO (http://www.cloudsat.cira.colostate.edu/, accessed on 10 November 2023) is equipped with a Cloud Aerosol Lidar with Orthogonal Polarization (CALIOP). The CPR can penetrate thicker cloud layers, whereas CALIOP is better suited for detecting the microphysical characteristics of thin upper-level ice clouds. The two satellites, with their close temporal spacing, complement each other in observing the vertical distribution of clouds and other hydrometeors on a global scale [29,30]. Due to the operational status of CloudSat, data are available from 2007 to 2016; however, there was a hiatus in 2011–2012 because of battery issues, and after 2012, it has been limited to daytime data collection [31]. Since only two tracks pass over the Tibetan Plateau at the same local solar time each day (one during the day and one at night), the satellite's revisit time is approximately 14 days, and it does not achieve complete coverage of the entire plateau region.

The cloud-type product (2B-CLDCLASS-LIDAR) released by CloudSat combines the detection results of CPR and CALIOP. It also incorporates select data from Aqua/MODIS and temperature profiles from the European Centre for Medium-Range Weather Forecasts (ECMWF) as auxiliary data to achieve accurate cloud classification [32]. This product includes physical quantities such as cloud phase, cloud type, cloud top height (CTH), cloud base height (CBH), and cloud thickness (CT). The retrieval method for cloud phase employs a reflectivity threshold approach based on temperature to classify clouds into ice clouds, water clouds, and mixed-phase clouds [33]. This method integrates the detection results from both CPR and CALIOP: when the cloud top temperature is below -38.5 °C, the cloud is classified entirely as ice; when the cloud top temperature is above -4 °C, it is classified entirely as water. For temperatures between these two thresholds, further discrimination is made using the attenuated backscatter coefficient from CALIOP and the radar reflectivity factor from CPR [34]. 2C-ICE mainly includes physical quantities related to ice clouds, such as ice effective radius (IER), IWC, and ice water path (IWP). The along-track resolution of the cloud product data is 2.5 km, with a cross-track resolution of 1.4 km. Each vertical profile consists of 125 layers, with a thickness of 240 m per layer.

ERA5 is the fifth generation of the atmospheric reanalysis dataset from The European Centre for Medium-Range Weather Forecasts (ECMWF), utilizing an assimilation system that incorporates several integrated forecasting systems specifically developed for reanalysis, resulting in improved data accuracy [35]. The dataset has a horizontal resolution of 31 km and extends vertically from the surface to 0.01 hPa (approximately 80 km above the surface) across 137 model levels. It covers the period from 1950 to the present and provides hourly atmospheric variable data. All ERA5 data products are freely available for download via the ECMWF Web API. This study employs daily average data for 2m_temperature and total column water vapor from the Tibetan Plateau region for the years 2007 to 2016, with a spatial resolution of $0.5^\circ \times 0.5^\circ$.

Based on CloudSat data availability, this study focuses on the ice cloud properties over the Tibetan Plateau (26°–40°N, 73°–104°E) using satellite data from daytime observations between 2007 and 2016 (missing 2011–2012). The orbital data were processed into gridded data with a resolution of $1^\circ \times 1^\circ$. Additionally, daily average data for surface temperature (2m_temperature) and total column water vapor from the ERA5 dataset for the same period (2007–2016, a total of 10 years) were used for background analysis. The spatial resolution of this data product is $0.5^\circ \times 0.5^\circ$. In this study, a masking method was applied to filter data

exclusively within the polygon representing the plateau for statistical analysis. Following the partitioning method outlined by Wang et al. [36], the plateau was divided into three sub-regions (see Figure 1): Region A in the western part (west of 90°E), Region B in the northeastern area (east of 90°E and north of 34°N), and Region C in the southeastern area (east of 90°E and south of 34°N). This classification primarily considers the differences in circulation backgrounds and elevation between the eastern and western parts of the plateau. In summer, the southern part of the plateau is mainly influenced by the Indian monsoon and the southwest monsoon, which bring abundant warm, moist air from the ocean, resulting in significant accumulation of moisture in the southern and southeastern regions of the plateau. In contrast, during the winter, the westerly wind belt predominantly affects the northern side of the plateau, where airflow is obstructed by the topography, splitting into southern and northern branches and forming a typical northern ridge and southern trough. As a result, the entire plateau and its northern areas are under the influence of intense subsiding airflow. The authors of [12,37] analyzed the distribution patterns of moisture and precipitation over the plateau and pointed out that the 300 mm precipitation line from May to September can serve as an indicator of the northern boundary of the Asian summer monsoon on the Tibetan Plateau. This boundary runs along the eastern Qilian Mountains–Tanggula Mountains–Qiangtang Plateau–Gangdise Mountains–Himalayas line, roughly between 30°N and 35°N, marking the convergence zone of the monsoon and westerly winds. The alternating control of the plateau by the summer monsoon and the westerly wind system leads to significant differences in moisture transport across the northern and southern boundaries of the plateau. This also contributes to the accumulation of dust aerosols in the Qaidam Basin (Region B), which significantly influences the formation and distribution of ice clouds. Therefore, this study investigates the characteristics of ice clouds in these three sub-regions during the warm and cold seasons, where the warm season includes May to September, and the cold season encompasses November to March.

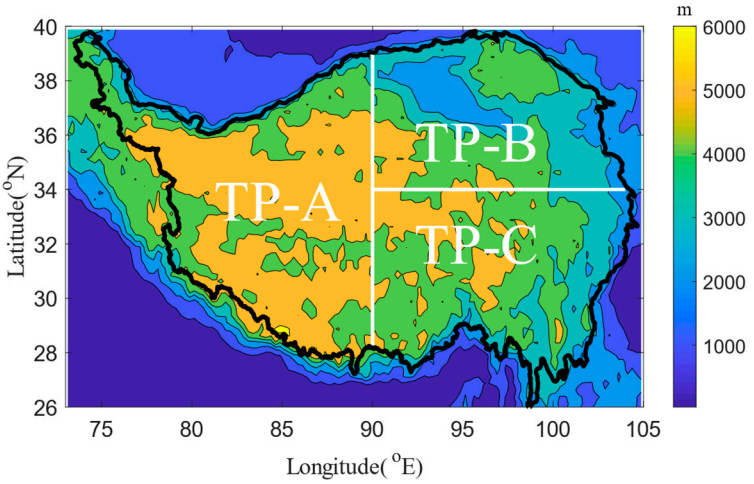


Figure 1. Regional division of the Tibetan Plateau.

3. Results

3.1. Distribution of Macrophysical Characteristics of Ice Clouds

3.1.1. Ice Cloud Occurrence Frequency

The occurrence and coverage of clouds to some extent reflect the climatic characteristics of a region, and different-phase clouds play varying roles in regulating the atmospheric radiation budget over land. Among these, the total cloud occurrence frequency (P_c) is equal to the ratio of the total number of cloud profiles (N_c) to the total number of radar scan profiles (N_{all}), the absolute occurrence frequency of ice clouds (P_{ice_ab}) is equal to the ratio of the number of ice cloud profiles (N_{ice}) to the total number of radar scan profiles, and the

relative occurrence frequency of ice clouds (P_{ice_re}) is equal to the ratio of the number of ice cloud profiles to the total number of cloud profiles, as follows:

$$P_c = N_c / N_{all} \times 100\%; \quad (1)$$

$$P_{ice_ab} = N_{ice} / N_{all} \times 100\%; \quad (2)$$

$$P_{ice_re} = N_{ice} / N_c \times 100\%. \quad (3)$$

Figure 2 presents the monthly variation in total cloud and ice cloud occurrence frequency over the TP in 2015 and calculates the absolute and relative proportions of ice clouds to comprehensively understand their contribution. Overall, there is more than 60% cloudy weather throughout the year, of which the highest occurrence frequency is around 87% in June and the lowest around 58% in December. It roughly presents a clear "convex" shape, indicating that the total cloud occurrence frequency is greater in the warm season. The change curve of the occurrence frequency of ice clouds is exactly the opposite, with their relative and absolute occurrence frequencies showing a "concave" shape, meaning that the cold season is greater than the warm season. The absolute proportion of ice clouds is the lowest in September, at around 38%, and the highest in April, at around 78%. The overall cold season remains around 60%, while the warm season is around 50%. During the warm season, the relative and absolute proportions of ice clouds are quite similar, while in the cold season, the relative proportion significantly exceeds the absolute proportion, ranging from around 80% to 90%. During the warm season, the plateau is primarily influenced by summer monsoons, which mainly produce convective clouds, resulting in a relatively lower contribution from ice clouds. In contrast, during the cold season, ice clouds play a dominant role. It also indicates that the size and variety of hydrometeors in the plateau are more diverse in the warm season compared to the cold season. A comprehensive comparison of the occurrence of total clouds and ice clouds reveals that the seasonal variation in ice clouds in the plateau region is greater than that in total clouds.

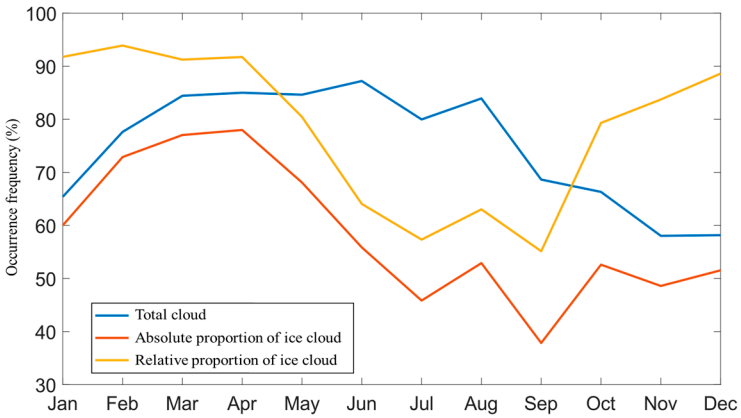


Figure 2. Monthly variations in total cloud and ice cloud occurrence frequency over the TP in 2015.

Based on the studies by Kukulies et al. (2019) and Wang et al. (2021) regarding the warm and cold season characteristics of ice clouds [17,28], as well as the distribution features of ice clouds in Figure 2, the classification of cold and warm seasons is shown to be representative. The ice clouds in the cold season and warm season from 2007 to 2016 were statistically analyzed as follows. Figure 3 shows the spatial distribution of the annual average relative occurrence frequency of ice clouds during the cold and warm seasons, revealing distinct seasonal variations and regional disparities in ice cloud distribution. The high-value area of ice clouds in the warm season is mainly concentrated over the west of the plateau, at around 60%. In contrast, during the cold season, ice cloud occurrence covers over 80% of the plateau area, indicating their predominant role during this period. Considering the changes in the circulation patterns of the TP, it can be observed that

during the warm season, the southern side of the plateau is primarily influenced by the Indian monsoon and the southwest monsoon, which carry abundant warm and moist air from the ocean. When this airflow encounters the topography, it is forced to rise, causing the high heat and humidity to condense and release latent heat. This results in frequent and intense convection and precipitation in the southern and southeastern regions of the plateau, leading to a predominance of water clouds, while ice clouds are relatively rare. During the cold season, the westerly wind belt passes over the plateau, shifting overall to the north. Additionally, the towering topography of the plateau obstructs these winds, causing the westerly flow to split into southern and northern branches, forming a typical northern ridge and southern trough. Consequently, the entire plateau and its northern areas are under the influence of strong subsiding airflow, resulting in mostly clear weather conditions and a predominance of ice clouds.

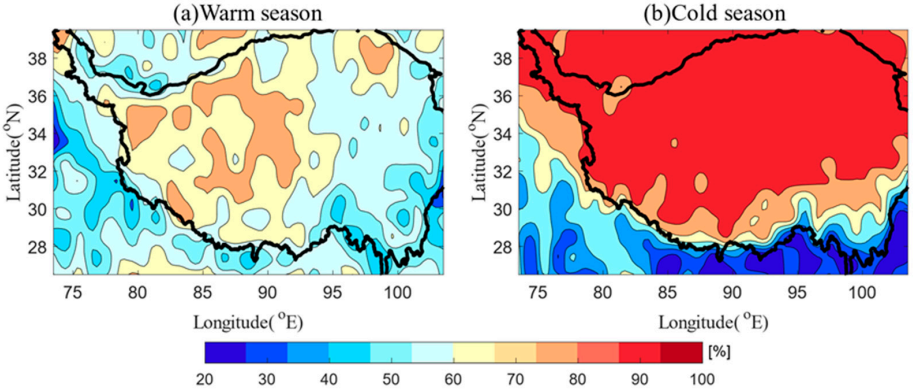


Figure 3. Spatial distribution of relative ice cloud occurrence frequency in cold and warm seasons from 2007 to 2016.

3.1.2. Ice Cloud Top Height, Base Height, and Thickness

Besides the impact of cloud occurrence frequency on terrestrial radiation, the position of clouds in the atmosphere also affects both the long- and shortwave radiation budgets and balances of the terrestrial and atmospheric systems. Accordingly, this section analyzes the probability density function (PDF) distributions of ice cloud CTH, CBH, and CT over various sub-regions of the TP during the cold and warm seasons from 2007 to 2016. The "height" of the cloud base or cloud top here is the actual height from the ground surface of the plateau, not the altitude.

Overall, there are significant seasonal variations in the distribution of ice cloud attributes across different sub-regions of the TP (Figure 4). Compared to the cold season, the PDF distributions of ice cloud CBH and CTH in the warm season exhibit flatter profiles, and both mean values are larger. The variation in CT in the cold and warm season is relatively small, with a slightly larger average in the warm season. The average CBH in the warm season ranges from 3 to 5 km across the three regions, whereas during the cold season it hovers around 2 km. Similarly, the CTH during the warm season ranges from approximately 5 to 8 km, while during the cold season it is around 4.5 km. The CT differences in the cold and warm seasons are minimal, averaging around 2 km in both seasons. Under conditions of abundant moisture, ice cloud formation in the warm season is likely primarily influenced by temperature, resulting in significantly higher occurrence heights compared to the cold season, along with relatively thicker ice cloud layers.

A comparative analysis of the three sub-regions within the plateau reveals significant disparities in the distribution of CTH and CBH during the warm season, whereas differences in distribution among the regions during the cold season are relatively minor. Specifically, regions A and B exhibit similar distribution characteristics during the warm season, which contrast significantly with those of region C. Except for the bimodal distribution of CBH in region C (0–2 km and 7–9 km), all others are unimodal distributions. Compared to regions A and B, the distribution range of CTH and CBH in warm season

region C is broader, with a relatively uniform proportion at different heights. The average CTH and CBH are the highest among the three regions. This shows that ice clouds form at various height levels in this area, and their distribution is relatively uniform. In the southeastern part of the plateau (region C), influenced by the South Asian monsoon, there is ample moisture, leading to frequent deep convective activities and the explosive growth of high-altitude cirrus clouds [38]. Therefore, compared to the western and northeastern parts of the plateau (regions A and B), the formation height of ice clouds in the southeastern part of the plateau is higher, likely due to the outflow from the tops of deep convective clouds causing the formation of upper-level ice clouds [39]. Additionally, region C exhibits the most significant seasonal variation, with the average CTH and CBH differing by 2.83 km between the cold and warm seasons, which are the highest among the three regions. The thickness of ice clouds shows relatively consistent distribution characteristics across sub-regions in both cold and warm seasons, with the frequency decreasing as cloud thickness increases in the warm season, while a peak frequency is observed at 1–2 km during the cold season.

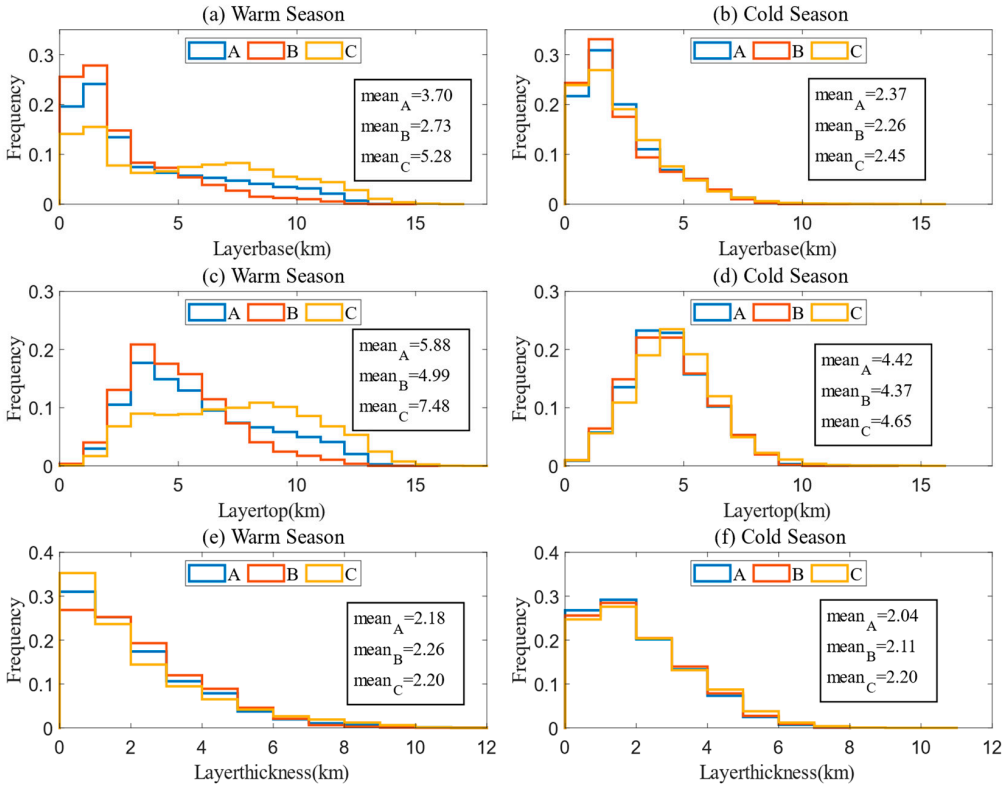


Figure 4. Statistical distribution of ice cloud top height, base height, and thickness in various sub-region of the TP from 2007 to 2016 (A, western region; B, northeast region; C, southeast region).

3.2. Distribution of Microphysical Characteristics of Ice Clouds

IWC and IER are two important parameters that describe the microphysical characteristics of ice clouds; plus, they also serve as two basic parameters reflecting the characteristics of ice clouds in radiation transfer models and climate models. Since the IWC values span several orders of magnitude, the IWC is logarithmic (L_{IWC}) and separated by 0.1, and the height is separated by 250 m. Then, the occurrence frequency count of particles in each interval is calculated. In addition, the IER is calculated at intervals of 0.5 μm, and the statistical method is the same as above.

3.2.1. Ice Water Content

The IWC reflects the mass of all ice crystals contained within the ice cloud and is an important parameter for describing the microphysical properties of ice clouds. Figure 5

shows the logarithmic annual average occurrence frequency count of the IWC in different regions of the plateau during the cold and warm seasons, as well as the variation in the logarithmic average IWC with height. Overall, the distribution of L_{IWC} in different regions of the plateau exhibits a triangular pattern, with a narrow upper and wide lower range, indicating that the distribution range of L_{IWC} at higher altitudes is relatively concentrated, while the distribution range of L_{IWC} at lower altitudes is relatively dispersed. Furthermore, there is a unique peak frequency count centered in the lower part of the "triangle". The average value of L_{IWC}, represented by white dotted lines, gradually decreases with increasing height, especially at the top of the graph, where its value decreases more rapidly. From a numerical perspective, the overall L_{IWC} of the plateau is mainly concentrated within the range of -1 to 3, with IWC ranging from 0 to 900 mg/m^3. L_{IWC} is mainly distributed in the warm season at 1–12 km, and in the cold season at 1–6 km.

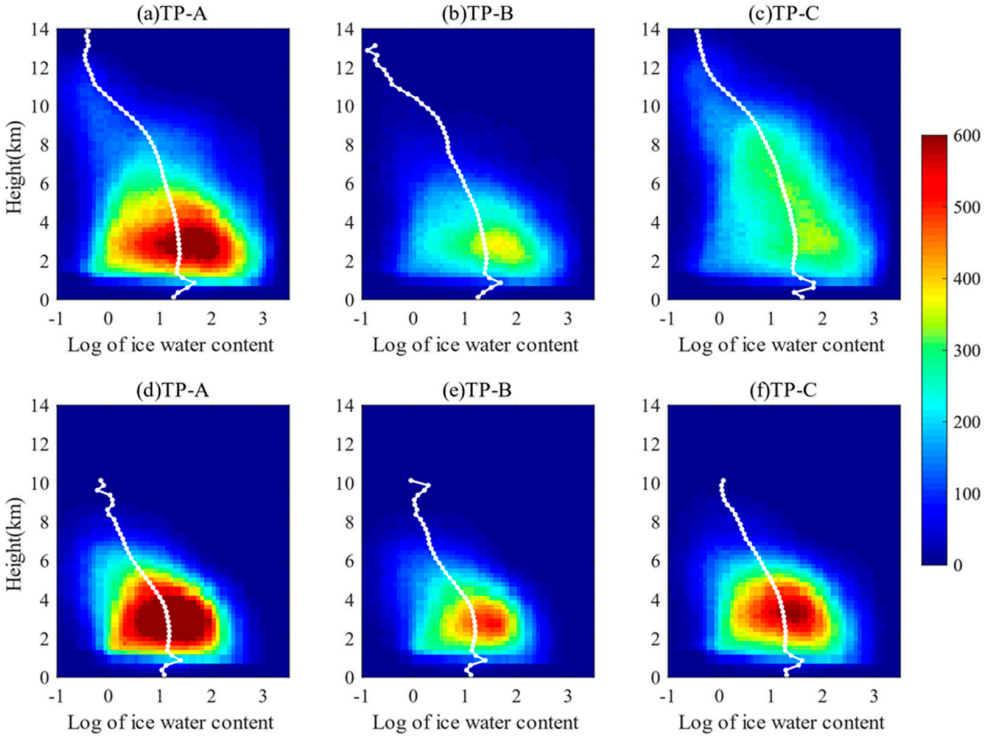


Figure 5. Distribution of annual mean occurrence frequency count of L_{IWC} with height in the (**a**–**c**) warm season and (**d**–**f**) cold season from 2007 to 2016. The white dotted lines in the figure represent the mean values at each height level.

All three regions show significant seasonal changes, and the frequency count of L_{IWC} occurrence is higher in the cold season. By comparing the three sub-regions, it is found that the frequency count of L_{IWC} is highest in the western region of the plateau (Figure 5a,d) and lowest in the northeast region (Figure 5b,e), which is influenced by the high terrain in the western region and promotes the formation of more ice clouds. In addition, the distribution of L_{IWC} in the southeastern region of the plateau during the warm season (Figure 5c) is relatively uniform with height, which coincides with the distribution of CTH and CBH in the region (Figure 4a,c).

3.2.2. Ice Cloud Effective Radius

The effective radius of particles has both area-weighted and volume-weighted characteristics and is commonly used to discuss the total volume or mass of particle clusters and their relationship with optical properties. It not only affects the scattering characteristics of clouds, but also further affects the microphysical processes in clouds. Figure 6 shows the variation in the annual occurrence frequency count of the IER with height in different

regions of the plateau, and the variation curve of the average effective radius with height is superimposed. From Figure 6, the IER of warm-season ice clouds on the plateau is mainly concentrated in the range of 10–90 μm, occurring at a height of approximately 1–12 km. The occurrence range of cold-season ice clouds is relatively small, with the IER mainly concentrated in the range of 20–70 μm from 1 to 8 km. The average IER decreases gradually with increasing altitude, regardless of the cold or warm season. The maximum value of the warm-season average IER in various regions of the plateau exceeds 65 μm, and the maximum value in the cold season does not exceed 60 μm. The study of various regions of the plateau reveals a significant characteristic in the distribution of IER with height: it has a narrow upper section and a wider lower section. The upper portion ranges from approximately 15 to 25 μm, while the lower portion spans multiple value units, ranging from around 20 to 85 μm. In the warm season, 7 km serves as a boundary, while in the cold season, 4 km is the dividing line. Overall comparison shows that, in the cold season, the frequency count of the IER is highest in the western region of the plateau (Figure 6d), concentrated at 1–8 km. In the warm season, meanwhile, the frequency count of ice crystal particles in the northeast region (Figure 6b) is lowest, indicating that the frequency of ice crystal particle formation in this region is extremely low.

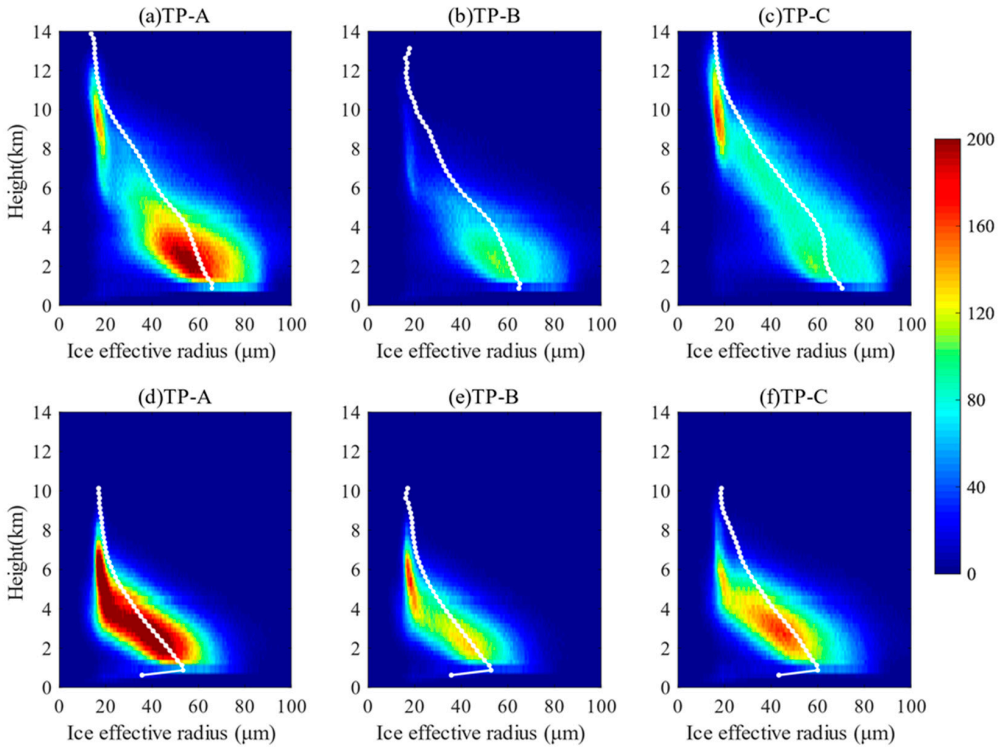


Figure 6. Distribution of annual mean occurrence frequency count of IER with height in the (**a**–**c**) warm season and (**d**–**f**) cold season from 2007 to 2016. The white dotted lines in the figure represent the mean values at each height level.

Compared with Figure 5, the spatial distribution of ice cloud IER and IWC has high consistency, especially after interval division, which is more conducive to the study of ice cloud parameterization [40]. From Figure 6a, it can be seen that there are two significant peak centers in the western part of the warm-season plateau, with 20 μm being the boundary line, located at 1–6 km and 8–12 km, respectively. However, Figure 5a only has an extreme center near 1–6 km, indicating that the vast majority of IWC is owned by ice crystal particles with larger centers (40–80 μm). As the height increases, for small particles (<20 μm), the numerical density of ice water significantly increases, but its cumulative IWC remains within a small range. Considering the distinct stratification of the IER during the warm season on the plateau, it is hypothesized that ice clouds in this region may primarily form

through two mechanisms [41]. Lower-layer ice clouds in the plateau are likely formed mainly by orographic lift, while upper-layer ice clouds are thought to arise from cirrus clouds that emerge from the tops of deep convection, with relatively uniform sizes of internal ice crystal particles.

4. Discussion

On the basis of the results presented in the previous section, we have gained a preliminary understanding of the macro- and micro-attributes of ice clouds over the TP. This section further analyzes the impact of significant warming and changes in water vapor on ice clouds in the plateau. To match the data products from CloudSat satellite observations, the surface temperature and water vapor data from ERA5 are also selected for the period from 2007 to 2016.

4.1. Significant Warming Phenomenon of the TP

In the context of global warming, the issue of warming in the Tibetan Plateau has generated extensive discussion. Therefore, it is essential to clarify the specific warming trends in the region by analyzing the surface temperature from ERA5 for the period of 2007 to 2016. Figure 7 shows the anomalous changes and linear trends in the surface temperature over the TP from 2007 to 2016. From Figure 7a,b, it can be found that the overall temperature anomaly of the plateau shows an upward trend, with a warming rate of 0.095 °C/yr in the cold season and 0.038 °C/yr in the warm season. The former is more than twice that of the latter, suggesting that the cold season plays a more important role in the annual warming of the plateau, which basically aligns with the research conclusion of Xu et al. [42]. In addition, there are significant differences in temperature changes in different regions of the plateau (Figure 7c,d). In the warm season, the southern part of the plateau shows a warming phenomenon, and the western part of the plateau shows the most significant warming, with a maximum of 0.17 °C/yr. In the cold season, there is a warming phenomenon in the eastern part of the plateau, with the northwest and southeast regions experiencing particularly significant warming, mostly exceeding 0.18 °C/yr, while a sporadic weak cooling phenomenon occurs in the southwest and northeast of the plateau.

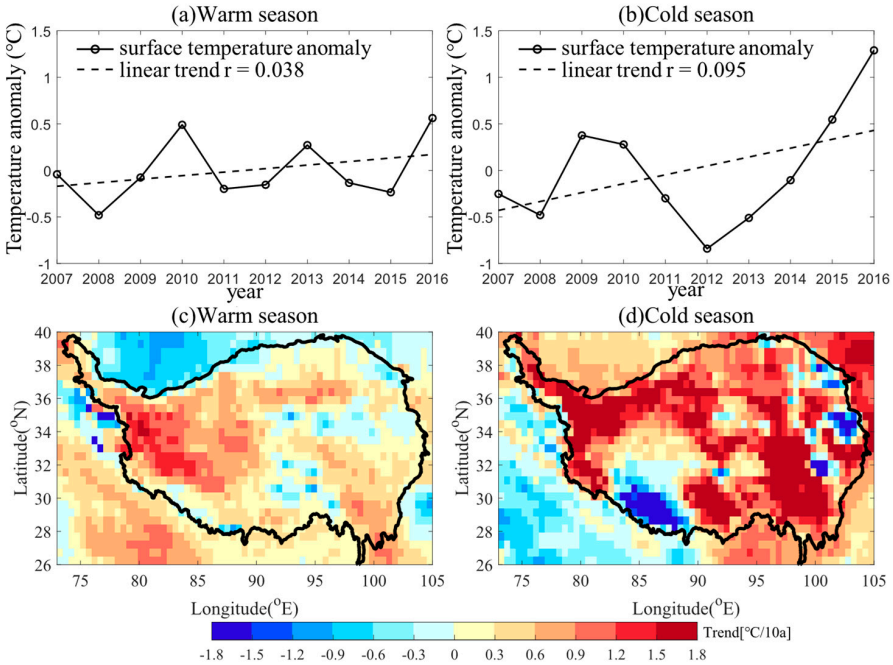


Figure 7. Linear trends in surface temperature anomalies in the (**a**) warm season and (**b**) cold season, and their distribution in the (**c**) warm season and (**d**) cold season from 2007 to 2016.

4.2. Changes in Water Vapor Content over the TP

As one of the key factors influencing cloud formation, the variation in water vapor during the study period may have significant implications for the changes in ice cloud properties. This study analyzes water vapor changes over the plateau using total column water vapor from ERA5 for the period of 2007 to 2016. Figure 8 shows the anomalous changes and linear trends in surface water vapor content over the TP from 2007 to 2016. From Figure 8a,b, it can be found that the water vapor has maintained a slow increase in the past decade, and the growth trend in the warm season is slightly greater than that in the cold season. The growth rate of water vapor in the warm season is around 0.012 mm/yr and around 0.006 mm/yr in the cold season. Further comparison of the changes in water vapor content over the plateau (Figure 8c,d) reveals that there is a water vapor reduction zone crossing the central part of the plateau during the warm season, while the water vapor content on both the north and south sides is increasing year by year, with a maximum of over 0.1 mm/yr. During the cold season, the water vapor content within the plateau shows a slow increasing trend on a large scale, with no more than 0.05 mm/yr. This is consistent with research by Chang et al. [43], which suggests that the increase in water vapor content over the plateau depends mainly on the increase in surface evaporation, while the actual water vapor transport is decreasing year by year.

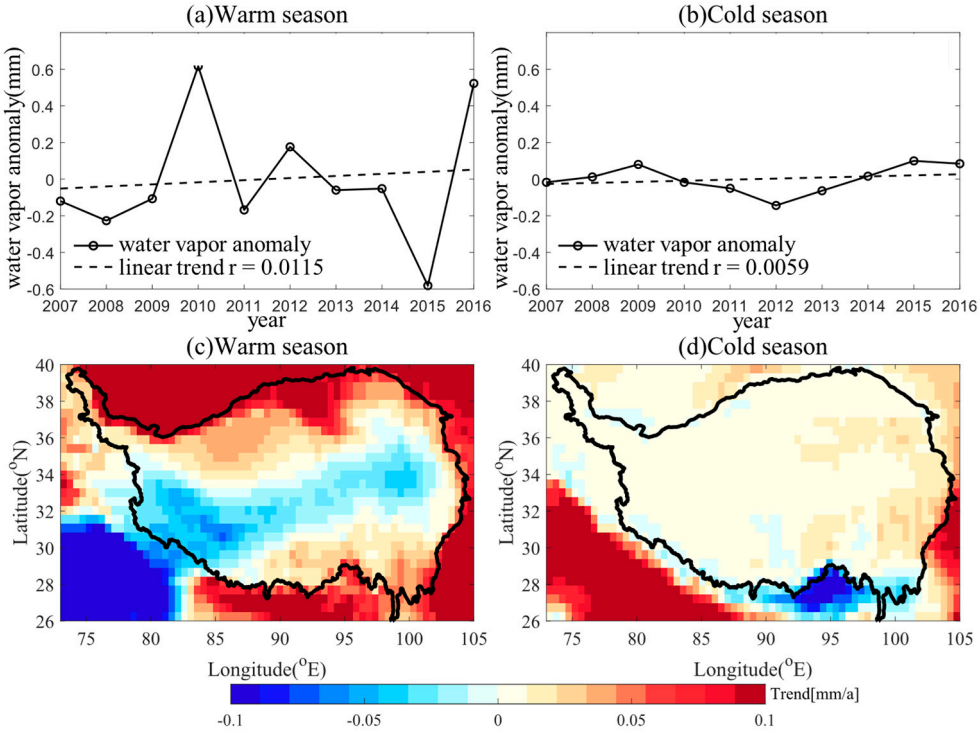


Figure 8. Linear trends in water vapor content anomalies in the (**a**) warm season and (**b**) cold season, and their distribution in the (**c**) warm season and (**d**) cold season from 2007 to 2016.

4.3. Changes in Ice Cloud Characteristics over the TP

According to the above research on the changes in temperature and water vapor over the plateau, this section further discusses the changes in ice clouds and their possible contribution to the plateau warming. Ice clouds are relatively transparent to incident solar shortwave radiation. When the ice cloud appears at a higher height and the optical thickness is smaller, it can capture more longwave radiation from the atmosphere and reflect less solar radiation, leading to a stronger greenhouse effect. As shown in Figure 4, the mean CT over the plateau is around 2 km. To study the changes in thin ice clouds and their effects on plateau warming, this section takes only single-layer ice clouds with a CT

of less than or equal to 3 km as the research object, accounting for around 80% of the total ice clouds.

Figure 9 shows the relative occurrence frequency of thin ice clouds over the TP from 2007 to 2016. The results indicate that there is a large-scale growth trend in ice clouds in both cold and warm seasons, and the growth of the former is obviously greater than that of the latter. In the warm season, ice cloud growth is primarily concentrated in the western and southeastern plateau, with a growth rate of around 0.5% per year, while in the cold season it is primarily concentrated in the western and northeastern plateau, with a maximum growth rate exceeding 3% per year. The distribution characteristics of ice clouds exhibit similar features to the spatial distribution of plateau warming, indicating a certain degree of influence by thin ice clouds on plateau warming, suggesting a potential correlation between the degree of surface temperature change and the frequency of thin ice clouds.

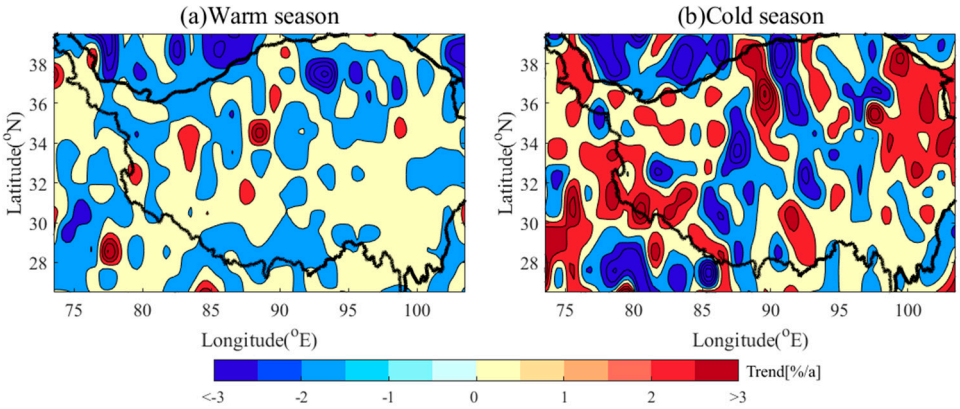


Figure 9. Spatial variation trend in the relative occurrence frequency of thin ice clouds in the cold and warm seasons over the TP from 2007 to 2016.

Figure 10 further analyzes the interannual changes in the characteristics of ice clouds and total clouds over the TP. According to the occurrence frequency of single-layer total clouds, it can be seen that the average annual proportion is around 55% in the warm season and around 51% in the cold season, both of which remain stable. While the total cloud occurrence frequency remains basically unchanged, the proportion of ice clouds is increasing year by year. In the warm season, the proportion of ice clouds is around 0.15% per year, while in the cold season it is more than 1% per year, around 10 times that of the warm season. The significant seasonal variation differences in ice clouds are highly consistent with the differences in plateau warming, fully suggesting that changes in thin ice clouds are closely related to variation during the cold season over the plateau.

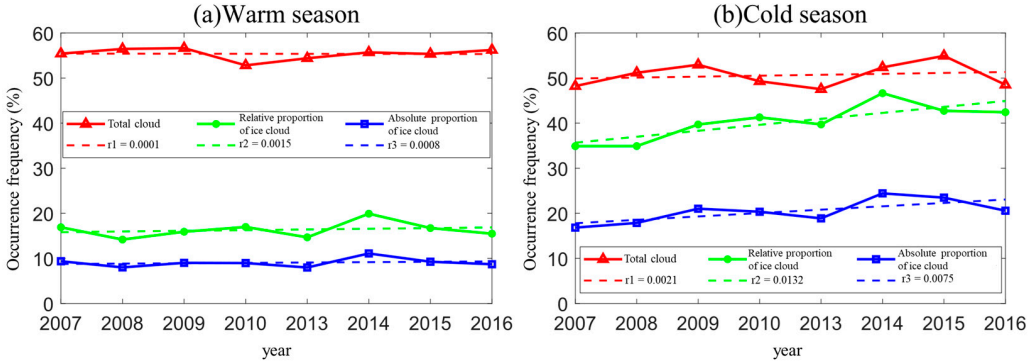


Figure 10. Interannual variation in the occurrence frequency of thin ice clouds in the cold and warm seasons over the TP from 2007 to 2016.

By comprehensively analyzing the changes in temperature, water vapor, and ice clouds (Figure 11), it can be found that the growth rate of water vapor over the plateau is greater in the warm season than in the cold season, while the growth rates of temperature and ice cloud occurrence are opposite. The results suggest that the surface temperature change may be related to the occurrence frequency of thin ice clouds, and a significant increase in surface temperature during the cold season may be related to the significant increase in the occurrence frequency of thin ice clouds. In addition, the water vapor growth in northeast China (region B) during the warm season is around 3% per year, but the ice cloud growth is negative. In the cold season, the water vapor growth in the western region (region A) is less than 0.5% per year, but the ice cloud growth exceeds 1% per year, suggesting that water vapor is not a direct factor in the increase in the incidence of thin ice clouds over the plateau.

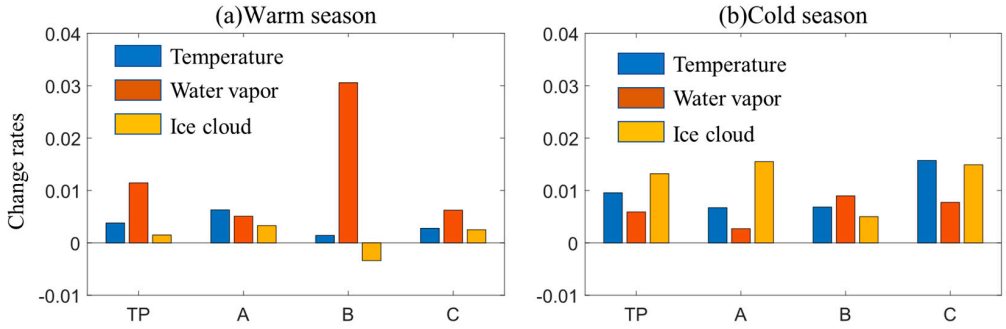


Figure 11. Comparison of rates of change in temperature, water vapor, and ice clouds during the (**a**) warm and (**b**) cold seasons of the TP and each sub-region.

5. Conclusions

This study utilizes CloudSat/CALIPSO satellite data from 2007 to 2016 to systematically investigate the optical and physical distribution characteristics of ice clouds in the Tibetan Plateau as a whole and in its sub-regions. Additionally, using ERA5 reanalysis data, the study analyzes the variations in surface temperature, water vapor, and ice clouds in the plateau region, researching the interactions between warming in the plateau and ice clouds. The major conclusions can be summarized as follows:

(1) The macro-properties of ice clouds exhibit significant seasonal variation and regional differences. In the plateau region, the frequency of ice cloud occurrence is higher in the cold season than in the warm season, with the relative proportion of ice clouds exceeding 80% in most areas during the cold season, compared to around 60% in the warm season. This indicates that ice clouds have a dominant presence in the cold season. In the warm season, the average CBH of ice clouds across the plateau regions is approximately 3 to 5 km, while in the cold season it is around 2 km. The average CTH in the warm season ranges from 5 to 8 km, compared to around 4.5 km in the cold season. The CH shows little variation between the two seasons, remaining around 2 km. Additionally, influenced by the background of plateau circulation and the topographical differences between the east and west, the southeastern part of the plateau exhibits more pronounced seasonal differences compared to the western and northeastern regions, with the highest disparities in average CTH and CBH between the cold and warm seasons among the three areas.

(2) Statistical analysis of the microphysical characteristics of ice clouds shows that IWC was found to be highly correlated with the spatial distribution of IER over the plateau. Generally, during the warm season, IWC and IER are predominantly distributed within the altitudinal range of 1–12 km above ground level, whereas during the cold season they are distributed within the range of 1–8 km, with overall higher occurrence frequencies during the cold season. The frequency is highest in the western plateau and minimum in the northeastern plateau. IWC mainly ranges from 10^{-1} to 10^{-3} mg/m^3, with a distribution pattern characterized by a triangular shape, with the peak values centered in the lower portion of the distribution. IER mainly distributes in the range of 10–90 μm, with one or

two peaks in occurrence frequency with altitude and one peak typically near 20 μm. The significant stratification of IER with height suggests that ice clouds in the plateau region may form through two different mechanisms.

(3) In the TP region, from 2007 to 2016, both surface air temperature and water vapor exhibited varying degrees of growth. The temperature increase was particularly notable, with a warming rate of approximately 0.038 °C/yr during the warm season and around 0.095 °C/yr during the cold season. In contrast, water vapor experienced a more gradual increase, with a warm-season rate of increase of around 0.012 mm/yr and a cold-season rate of approximately 0.006 mm/yr. Against the backdrop of significant warming over the plateau, the occurrence frequency of thin ice clouds has been increasing annually, with a warm-season annual growth rate of around 0.15% per year and a substantial 1% per year increase during the cold season. Through comprehensive comparison of the rates of change in temperature, water vapor, and ice clouds, it was found that the warm-season rate of increase in water vapor over the plateau surpasses that of the cold season, while the rates of increase in surface temperature and ice cloud occurrence frequency are both lower than those during the cold season. This suggests a potential correlation between the degree of surface temperature change and the frequency of thin ice clouds, with the significant increase in cold-season temperatures possibly linked to a corresponding increase in the occurrence frequency of thin ice clouds.

Author Contributions: Conceptualization, Y.G., X.W. and Z.Z.; methodology, J.H.; software, M.D.; validation, Z.Z. and X.Z.; writing—original draft preparation, Y.G., X.W. and Z.Z.; writing—review and editing, J.H.; visualization, Z.Z. and X.Z.; supervision, M.D.; project administration, X.W.; funding acquisition, J.H. All authors have read and agreed to the published version of the manuscript.

Funding: This research was funded by the National Key Research and Development Program of China (grant no. 2023YFC3010702); the General Program of the National Natural Science Foundation of China (grant no. 42275081); the Strategy Priority Research Program of Chinese Academy of Sciences (grant no. XDB0760100); the Project of China—Sri Lanka Joint Center for Education and Research, CAS (grant no. 133244KYSB20210026).

Data Availability Statement: The original contributions presented in the study are included in the article, further inquiries can be directed to the corresponding author.

Conflicts of Interest: Author Yating Guan was employed by the company Aerospace Newsky Technology Co., Ltd. The remaining authors declare that the research was conducted in the absence of any commercial or financial relationships that could be construed as a potential conflict of interest. The authors declare no conflict of interest.

References

1. Cess, R.D.; Potter, G.L.; Blanchet, J.P.; Boer, G.J.; Ghan, S.J.; Kiehl, J.T.; Le Treut, H.; Li, Z.-X.; Liang, X.-Z.; Mitchell, J.F.B.; et al. Interpretation of cloud-climate feedback as produced by 14 atmospheric general circulation models. *Science* **1989**, *245*, 513–516. [CrossRef] [PubMed]
2. Wang, F.; Ding, Y. An Evaluation of Cloud Radiative Feedback Mechanisms in Climate Models. *Adv. Earth Sci.* **2005**, *20*, 207–215.
3. Sassen, K.; Wang, Z.; Liu, D. Global distribution of cirrus clouds from CloudSat/Cloud-Aerosol Lidar and Infrared Pathfinder Satellite Observations (CALIPSO) measurements. *J. Geophys. Res. Atmos.* **2008**, *113*, D00A12. [CrossRef]
4. Liou, K.N. Influence of Cirrus Clouds on Weather and Climate Processes—A Global Perspective. *Mon. Weather Rev.* **1986**, *114*, 1167–1199. [CrossRef]
5. Hartmann, D.L.; Ockertbell, M.E.; Michelsen, M.L. The Effect of Cloud Type on Earths Energy-Balance—Global Analysis. *J. Clim.* **1992**, *5*, 1281–1304. [CrossRef]
6. Hong, G.; Yang, P.; Baum, B.A.; Heymsfield, A.J.; Xu, K.-M. Parameterization of Shortwave and Longwave Radiative Properties of Ice Clouds for Use in Climate Models. *J. Clim.* **2009**, *22*, 6287–6312. [CrossRef]
7. Liou, K.N.; Ou, S.S.; Takano, Y.; Roskovensky, J.; Mace, G.G.; Sassen, K.; Poellot, M. Remote sensing of three-dimensional inhomogeneous cirrus clouds using satellite and mm-wave cloud radar data. *Geophys. Res. Lett.* **2002**, *29*, 74-1–74-4. [CrossRef]
8. Parry, M.L.; Canziani, O.; Palutikof, J.P.; van der Linden, P.J.; Hanson, C.E. *Intergovernmental Panel on Climate Change. Climate Change 2007: Impacts, Adaptation and Vulnerability: Contribution of Working Group II to the Fourth Assessment Report of the Intergovernmental Panel on Climate Change*; Cambridge University Press: Cambridge, UK, 2007; p. 976.
9. Jakob, C. *Ice Clouds in Numerical Weather Prediction Models: Progress, Problems, and Prospects*; Oxford Academic: New York, NY, USA, 2002.

10. Waliser, D.E.; Li, J.L.; Woods, C.P.; Austin, R.T.; Bacmeister, J.; Chern, J.; Del Genio, A.; Jiang, J.H.; Kuang, Z.; Meng, H.; et al. Cloud ice: A climate model challenge with signs and expectations of progress. *J. Geophys. Res. Atmos.* **2009**, *114*, D00A21. [CrossRef]
11. Duan, A.M.; Wu, G.X. Role of the Tibetan Plateau thermal forcing in the summer climate patterns over subtropical Asia. *Clim. Dyn.* **2005**, *24*, 793–807. [CrossRef]
12. Yang, K.; Wu, H.; Qin, J.; Lin, C.; Tang, W.; Chen, Y. Recent climate changes over the Tibetan Plateau and their impacts on energy and water cycle: A review. *Glob. Planet. Chang.* **2014**, *112*, 79–91. [CrossRef]
13. Wu, G.X.; Liu, Y.M.; He, B.; Bao, Q.; Wang, Z. Review of the impact of the Tibetan Plateau sensible heat driven air-pump on the Asian summer monsoon. *Chin. J. Atmos. Sci.* **2018**, *42*, 488–504. (In Chinese) [CrossRef]
14. Tang, M.C. Some advances on the research of plateau monsoons (a review). *Plateau Meteor.* **1993**, *12*, 95–101. (In Chinese)
15. Zhao, Y.F.; Wang, D.H.; Yin, J.F. A study on cloud micropysical characteristics over the Tibetan Plateau using CloudSat data. *J. Trop. Meteor.* **2014**, *30*, 239–248. (In Chinese) [CrossRef]
16. Liu, J.J.; Chen, B.D. Cloud occurrence frequency and structure over the qinghai-tibetan plateau from CloudSat observation. *Plateau Meteor.* **2017**, *36*, 632–642. (In Chinese) [CrossRef]
17. Kukulies, J.; Chen, D.; Wang, M. Temporal and spatial variations of convection and precipitation over the Tibetan Plateau based on recent satellite observations. Part I: Cloud climatology derived from CloudSat and CALIPSO. *Int. J. Climatol.* **2019**, *39*, 5396–5412. [CrossRef]
18. Ma, X.B.; Li, D.L. Analyses on air temperature and its abrupt change over qinghai-xizang plateau in modern age. *Plateau Meteor.* **2003**, *22*, 507–512. (In Chinese)
19. Wang, X.; Yang, M.; Liang, X.; Pang, G.; Wan, G.; Chen, X.; Luo, X. The dramatic climate warming in the Qaidam Basin, northeastern Tibetan Plateau, during 1961–2010. *Int. J. Climatol.* **2014**, *34*, 1524–1537. [CrossRef]
20. You, Q.L.; Kang, S.C.; Li, J.D.; Chen, D.L.; Zhai, P.M.; Ji, Z.M. Several research frontiers of climate change over the Tibetan Plateau. *J. Glaciol. Geocryol.* **2021**, *43*, 885–901. (In Chinese) [CrossRef]
21. Chen, B.; Chao, W.C.; Liu, X. Enhanced climatic warming in the Tibetan Plateau due to doubling CO_2: A model study. *Clim. Dyn.* **2003**, *20*, 401–413. [CrossRef]
22. Duan, A.M.; Wu, G.X. Change of cloud amount and the climate warming on the Tibetan Plateau. *Geophys. Res. Lett.* **2006**, *33*, L22704. [CrossRef]
23. Pan, Z.X.; Mao, F.Y.; Gong, W.; Min, Q.; Wang, W. The warming of Tibetan Plateau enhanced by 3D variation of low-level clouds during daytime. *Remote Sens. Environ.* **2017**, *198*, 363–368. [CrossRef]
24. Bao, S.H.; Letu, H.; Zhao, J.; Shang, H.; Lei, Y.; Duan, A.; Chen, B.; Bao, Y.; He, J.; Wang, T.; et al. Spatiotemporal distributions of cloud parameters and their response to meteorological factors over the Tibetan Plateau during 2003–2015 based on MODIS data. *Int. J. Climatol.* **2019**, *39*, 532–543. [CrossRef]
25. Matus, A.V.; L'Ecuyer, T.S. The role of cloud phase in Earth's radiation budget. *J. Geophys. Res. Atmos.* **2017**, *122*, 2559–2578. [CrossRef]
26. Wang, M.H.; Su, J.; Xu, Y.; Han, X.; Peng, N.; Ge, J. Radiative contributions of different cloud types to regional energy budget over the SACOL site. *Clim. Dyn.* **2023**, *61*, 1697–1715. [CrossRef]
27. Hua, S.; Liu, Y.Z.; Jia, R.; Chang, S.; Wu, C.; Zhu, Q.; Shao, T.; Wang, B. Role of clouds in accelerating cold-season warming during 2000–2015 over the Tibetan Plateau. *Int. J. Climatol.* **2018**, *38*, 4950–4966. [CrossRef]
28. Wang, J.; Jian, B.D.; Wang, G.Y.; Zhao, Y.; Li, Y.; Letu, H.; Zhang, M.; Li, J. Climatology of Cloud Phase, Cloud Radiative Effects and Precipitation Properties over the Tibetan Plateau. *Remote Sens.* **2021**, *13*, 363. [CrossRef]
29. Stephens, G.L.; Vane, D.G.; Boain, R.J.; Mace, G.G.; Sassen, K.; Wang, Z.; Illingworth, A.J.; O'Connor, E.J.; Rossow, W.B.; Durden, S.L.; et al. The cloudsat mission and the a-train—A new dimension of space-based observations of clouds and precipitation. *Bull. Am. Meteorol. Soc.* **2002**, *83*, 1771–1790. [CrossRef]
30. Mace, G.G.; Zhang, Q.Q.; Vaughan, M.; Marchand, R.; Stephens, G.; Trepte, C.; Winker, D. A description of hydrometeor layer occurrence statistics derived from the first year of merged Cloudsat and CALIPSO data. *J. Geophys. Res. Atmos.* **2009**, *114*, D00A26. [CrossRef]
31. Nayak, M.; Witkowski, M.M. CloudSat Anomaly Recovery and Operational Lessons Learned. In Proceedings of the SpaceOps 2012, Stockholm, Sweden, 11–15 June 2012.
32. Wang, Z.; Vane, D.; Stephens, G.; Reinke, D.; TBD. *Level 2 Combined Radar and Lidar Cloud Scenario Classification Product Process Description and Interface Control Document*; California Institute of Technology Jet Propulsion Laboratory Report; California Institute of Technology Jet Propulsion Laboratory: Pasadena, CA, USA, 2012; p. 61.
33. Zhang, D.M.; Wang, Z.E.; Liu, D. A global view of midlevel liquid-layer topped stratiform cloud distribution and phase partition from CALIPSO and CloudSat measurements. *J. Geophys. Res. Atmos.* **2010**, *115*, D00H13. [CrossRef]
34. Wang, Z.; Sassen, K. Cloud type and macrophysical property retrieval using multiple remote sensors. *J. Appl. Meteoro.* **2001**, *40*, 1665–1682. [CrossRef]
35. Hersbach, H.; Bell, B.; Berrisford, P.; Hirahara, S.; Horányi, A.; Muñoz-Sabater, J.; Nicolas, J.; Peubey, C.; Radu, R.; Schepers, D.; et al. The ERA5 global reanalysis. *Q. J. Roy. Meteor. Soc.* **2020**, *146*, 1999–2049. [CrossRef]
36. Wang, T.H.; Han, Y.; Huang, J.P.; Sun, M.; Jian, B.; Huang, Z.; Yan, H. Climatology of Dust-Forced Radiative Heating over the Tibetan Plateau and Its Surroundings. *J. Geophys. Res. Atmos.* **2020**, *125*, e2020JD032942. [CrossRef]

37. Huang, L.X.; Chen, J.; Yang, K.; Yang, Y.; Huang, W.; Zhang, X.; Chen, F. The northern boundary of the Asian summer monsoon and division of westerlies and monsoon regimes over the Tibetan Plateau in present-day. *Sci. China Earth Sci.* **2023**, *66*, 882–893. [CrossRef]
38. Kukulies, J.; Chen, D.; Curio, J. The role of mesoscale convective systems in precipitation in the Tibetan Plateau region. *J. Geophys. Res. Atmos.* **2021**, *126*, e2021JD035279. [CrossRef]
39. Wang, K.; Chen, J.; Hong, Z.C.; Yan, C.Q.; He, Q.S. Research of the Distribution Characteristics and Generation Mechanism of Cirrus Clouds over the Qinghai-Xizang Plateau in Summer. *Plateau Meteor.* **2023**, *42*, 543–552. (In Chinese) [CrossRef]
40. Liou, K.N.; Gu, Y.; Yue, Q.; McFarguhar, G. On the correlation between ice water content and ice crystal size and its application to radiative transfer and general circulation models. *Geophys. Res. Lett.* **2008**, *35*, L13805. [CrossRef]
41. Zhao, C.F.; Liu, L.P.; Wang, Q.Q.; Qiu, Y.; Wang, W.; Wang, Y.; Fan, T. Toward understanding the properties of high ice clouds at the Naqu site on the Tibetan Plateau using ground-based active remote sensing measurements obtained during a short period in July 2014. *J. Appl. Meteorol. Clim.* **2016**, *55*, 2493–2507. [CrossRef]
42. Xu, Y.M.; Knudby, A.; Ho, H.C.; Shen, Y.; Liu, Y. Warming over the Tibetan Plateau in the last 55 years based on area-weighted average temperature. *Reg. Environ. Chang.* **2017**, *17*, 2339–2347. [CrossRef]
43. Chang, S.T.; Liu, Y.Z.; Hua, S.; Jia, R. Characteristics of atmospheric water vapor over the Qinghai-Tibetan plateau in summer with global warming. *Plateau Meteor.* **2019**, *38*, 227–236. (In Chinese) [CrossRef]

Disclaimer/Publisher's Note: The statements, opinions and data contained in all publications are solely those of the individual author(s) and contributor(s) and not of MDPI and/or the editor(s). MDPI and/or the editor(s) disclaim responsibility for any injury to people or property resulting from any ideas, methods, instructions or products referred to in the content.